Proceedings of the 7th International Symposium on Cavitation
CAV2009
August 17-22, 2009, Ann Arbor, Michigan, USA

CAV2009 – Paper No. 9

Unsteady Dynamics of Cloud Cavitating Flows around a Hydrofoil

Guoyu Wang
Email: wangguoyu@bit.edu.cn
Beijing Institute of Technology, China

Bo Zhang
Email: wangguoyu@bit.edu.cn
Beijing Institute of Technology, China

Biao Huang
Email: wangguoyu@bit.edu.cn
Beijing Institute of Technology, China

Mindi Zhang
Email: wangguoyu@bit.edu.cn
Beijing Institute of Technology, China

ABSTRACT

The unsteady dynamics of cloud cavitating flow around a hydrofoil are investigated by joint experimental and numerical methods. Experiments are carried out in a rectangular test section of a cavitation tunnel. A high-speed video camera is used to visualize the unsteady flow structures. The visualized data are analyzed by using a home made soft ware. The drag and lift under the cavitation condition are measured. The spectral analysis for the measured date is conducted. The computations are conducted on the two-dimensional hydrofoil section, based on a single-fluid model of the cavitation: the liquid/vapor mixture is considered as a homogeneous fluid whose composition is regulated by mass transfer equation. The RNG $k-\varepsilon$ turbulence model with modified eddy viscosity coefficient is used for the computations, and the modified coefficient is related to the vapor and liquid densities in cavitated regions for simulating the cavitating flow. A good agreement is obtained between experimental data and numerical simulations. The cloud cavitating area is divided in two parts: attached vapor sheet in the foreside of the cavity, and unsteady two-phase mixture in the rear region in the process of cavity breaking off. The local pressure increasing induced by the re-entrant jet is the main reason to lead the cloud cavity. The adverse pressure gradient in the rear area of the cavity is mainly responsible for the generation of the re-entrant jet.

INTRODUCTION

Cavitation occurs in a wide variety of engineering systems: pumps, hydrofoils and underwater bodies. In certain cavitation number conditions, all the vaporized area becomes unstable with periodical shedding of large bubble cluster. This cavitation configuration is usually called cloud cavitation. Phenomenological, cloud cavitation often involves complex interactions of turbulence and phase-change dynamics, large density variation between phases, fast and multiple time scales, and pressure fluctuations, which is responsible for several instabilities that affect the global behavior of the hydraulic systems. For example, in rocket engine turbopump, cloud cavitation is associated with severe vibrations that may lead to blade destruction. The physical mechanisms of self-oscillatory behaviour of the cloud cavitation are not well understood due to the complex, unsteady flow structures associated with cavitation dynamics and turbulence.

In the last decade or two, various advanced experimental techniques have been developed to study the physical mechanisms and flow structures of the cloud around a hydrofoil. Up to now, most of the work point out a re-entrant jet that flows under the cavity from its rear part to its upstearm end. When this jet reaches the caivity sheet interface, the cavity breaks off and its downstream part is converted by the main flow[1]. Furness and Hutton[2] first suggest that re-entrant jet is the principal mechanism if cloud cavitation, which is confirmed by Kubota et al.[3], Le et al.[4] and Kawanami et al.[5]. More over, the occurrence of the re-entrant jet has led to several conjectures: Callenaere point out that the adverse pressure gradient in the cavity wake plays an impotant role in the progression [6]. Gopalan and Katz find that the collapse of vapor cavities in the closure region of attached cavitation is the primary mechanism of vorticity production [7]. More generally, Leroux et al. measured the pressure distribution in partial cavitation, and discussed the unsteady characteristics [8]. Wang et al. provided the dynamics of attached cavitation, imposing

the evolvement of cavitation vortices under various cavitation regimes [9].

On the computational modeling side, unsteady Navier-Stokes equations-based techniques have been developed to simulate cavitation characteristics, including pressure, velocity, and phase change characteristics. Alternative computational modeling approaches have been proposed. These studies can be classified into two categories, namely, interface tracking methods [10] and homogeneous equilibrium flow models. Here, we concentrate on the homogeneous modeling approach. Reviews of this approach can be found in the references [11]. Based on the homogeneous equilibrium flow theory, the mixture concept can be introduced, and mass and momentum equations along with turbulence and cavitation models can be established for the entire flow field. Specifically, two approaches have been utilized to model the cavitation dynamics. The first one is the arbitrary barotropic equation model, which suggests that the relationship between density and pressure is $\rho = f(p)$, and the second one is the transport equation-based model (TEM). Barotropic equations were proposed by Delannoy and Kueny [12]. They assumed that density is a continuous function of pressure where both pure phases were incompressible, and the phase change could be fitted by a sine curve. Arbitrary barotropic equation models (density is only a function of pressure) can't capture baroclinic vorticity production because the baroclinic term of the vorticity transport equation yields zero by definition [13]. Consistent with the experimental study [7], Senocak and Shyy have demonstrated computationally that the baroclinic vorticity generation is important in the closure region [14]. In the TEM, a transport equation for either mass or volume fraction, with appropriate source terms to regulate the mass transfer between vapor and liquid phases, is adopted. An advantage of this model comes from the convective character of the equation, which allows modeling of the impact of inertial forces on cavities like elongation, detachment and drift of cavity bubbles, especially in complex 3-D interface situations [9]. Numerically, Singhal et al. [15], and Wu et al. [10] utilized pressure-based algorithms, while Kunz et al. [16] employed the artificial compressibility method. For flows with large property variations and high Reynolds number, the convection treatments and the boundary treatment are of importance as well. Some of the issues regarding the convection treatment can be found in Shyy [13]. As for the turbulence model, different closures have been utilized to treat unsteady cavitating flows[17]. Since the high eddy viscosity in the standard k-ε model dampens the unsteady characteristics dramatically [18], alternative approaches have been adopted by modifying the eddy viscosity [19]. It seems that especially for unsteady flow computations,,satisfactory results more critically depend on the turbulence model.

The unsteady dynamics of cloud cavitating flow around a hydrofoil are investigated by joint experimental and numerical methods. A high-speed video camera is used to visualize the unsteady flow structures. The visualized data are analyzed by using a home made soft ware. The drag and lift under cloud cavitation conditions are measured. The spectral analysis for the measured date is conducted. The computations are conducted on the two-dimensional hydrofoil section, based on a single-fluid model of the cavitation: the liquid/vapor mixture is considered as a homogeneous fluid whose composition is regulated by mass transfer equation. The RNG $\kappa-\varepsilon$ turbulence model with modified eddy viscosity coefficient is used for computing, and the modified coefficient is related to the vapor and liquid densities in cavitated regions for simulating the cavitating flow. Based on the computational and experimental results, several key problems related to the unsteady dynamics of cloud cavitating flows are address.

EXPERIMENTAL APPROACH

The experiments are carried out in a closed-loop cavitation tunnel,as show in Figure 1. A tank with a volume of $5m^3$ is placed upstream of the test section to separate undesired free stream bubbles. The top of the tank is connected to a vacuum pump for controlling the pressure in the tunnel. Between the test section and the tank, a corner vane and a straightening vane are used to reduce the turbulence level of the flow in the test section. The detailed position of a hydrofoil located in the test section, with 10c in length, 2.7c in height and 1c in width, is given in Figure 2. The flowing patterns can be observed from three windows, one on the top, one on the bottom and one on the side, which are made of perspex for optical access. In the whole test section, the average velocities are well-distributed, and the turbulence intensity levels are smaller than 2%. The cavitation number is controlled to within 5% uncertainty.

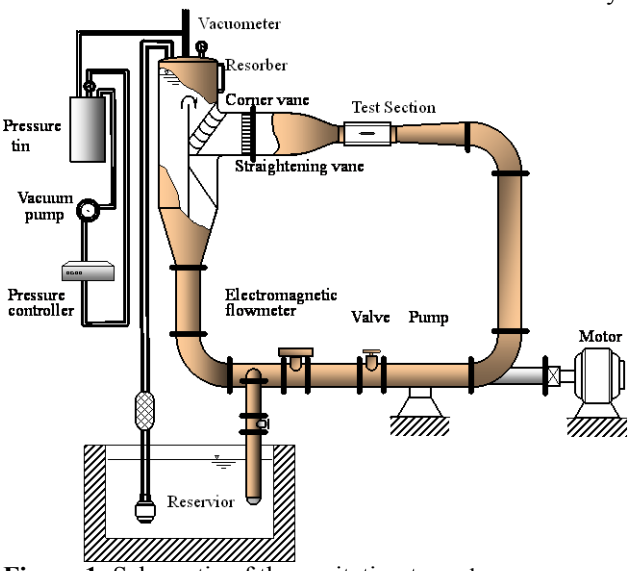

Figure 1: Schematic of the cavitation tunnel

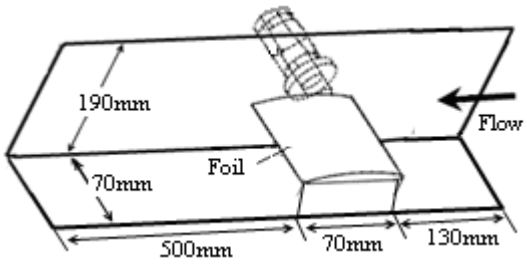

Figure 2: Geometries of the test section

In this study, the reference velocity U_∞ is fixed at 10m/s, the cavitation number, the Reynolds number *Re* and the lift/drag coeffieient are defined:

$$\sigma = \frac{p_\infty - p_v}{\frac{1}{2}\rho U_\infty^{\ 2}} \quad (1)$$

$$Re = \frac{U_\infty C}{\mu_t} \quad (2)$$

$$C_p = \frac{p - p_\infty}{0.5\rho U_\infty^2} \quad (3)$$

$$C_l = \frac{F_y}{0.5\rho U_\infty^2 C} \quad (4)$$

$$C_d = \frac{F_x}{0.5\rho U_\infty^2 C} \quad (5)$$

A Clark-Y hydrofoil, as shown in Figure 3, is adopted in the present study. The hydrofoil, with $1C$ in spanwise direction, is made of stainless steel, and highly surface-polished. The suction side of the foil is mounted toward the bottom for the convenience of viewing the flowing field. The definition of incidence angle α is presented in Figure 4.

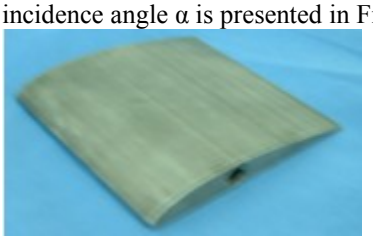

Figure 3: The picture of a Clark-y hydrofoil

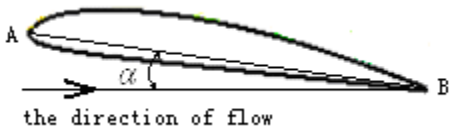

Figure 4: The definition of incidence angle

The cavitation phenomena are documented by a high-speed digital camera (HG-LE, by Redlake), up to a rate of 10^5 frames per second (fps). In order to maintain desirable spatial resolutions, much lower recording speed is adopted. Specifically, depending on the focus of the investigation, three rates, namely, 50, 2000, and 500 fps are used in this study, respectively. The experimental setup is illustrated in Figure 5.

The lift and drag are measured using a dynamic measure device in our laboratory,as show in Figure 6. Signals are amplified, filtered and collected through a 8-channel 16-bit A/D digitizer, at simultaneous sample with a maximum available sample frequency of 51.2 kHz. The control and the measurement data storage are performed by a PC. Finally, the signal processing is developed using MATLAB software.

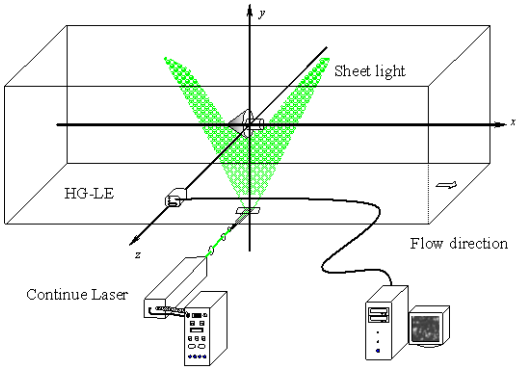

Figure 5: Schematic of the layout of the experimental setup

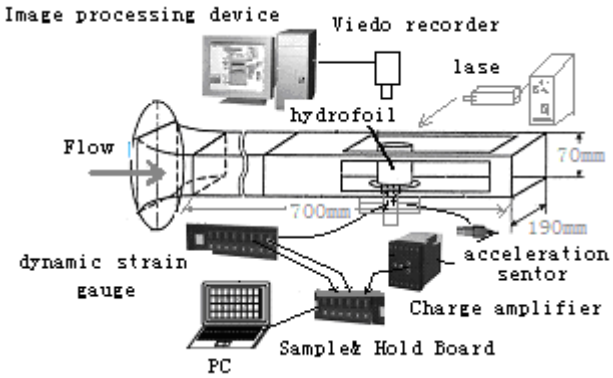

Figure 6: The schematic diagram of the dynamic measure system

COMPUTATIONAL APPROACH

Governing equations

The Favre averaged form of the mass conservation equation and Navier-Stokes equation for the momentum conservation are written in Cartesian co-ordinates:

$$\frac{\partial \rho}{\partial t} + \nabla \cdot (\rho \vec{u}) = 0 \quad (6)$$

$$\frac{\partial}{\partial t}(\rho \vec{u}) + \nabla \cdot (\rho \vec{u}\vec{u}) = -\nabla P + \nabla \cdot [(\mu + \mu_t)\nabla \vec{u}] + \frac{1}{3}\nabla[(\mu + \mu_t)\nabla \cdot \vec{u}] \quad (7)$$

here, $\rho = \rho_v \alpha_v + \rho_l (1 - \alpha_v)$ (8)

Turbulence model

The RNG k-ε model proposed by Yakhot et al. [20] is as follows:

$$\frac{\partial(\rho k)}{\partial t} + \nabla \bullet (\rho k \vec{u}) = \nabla \bullet \left[\left(\mu + \frac{\mu_t}{\sigma_{kRNG}} \right) \nabla k \right] + p_k - \rho\varepsilon \quad (9)$$

$$\frac{\partial(\rho\varepsilon)}{\partial t} + \nabla \bullet (\rho\varepsilon \vec{u}) = \nabla \bullet \left[\left(\mu + \frac{\mu_t}{\sigma_{\varepsilon RNG}} \right) \nabla \varepsilon \right] + \frac{\varepsilon}{k}(C_{\varepsilon 1RNG} p_k - C_{\varepsilon 2RNG} \rho\varepsilon) \quad (10)$$

where, the turbulent viscosity is defined as:

$$\mu_t = f(\rho) C_{\mu RNG} k^2/\varepsilon \tag{11}$$

It was observed that the RNG k-ε model resulted in shorter cavity lengths compared to the experiments[17]. Accordingly, a modified RNG k-ε turbulence closure model, proposed by Coutier-Delgosha et al.[17], is adopted in this study. Here, the major difference is the definition of the function $f(\rho)$. Compared to $f(\rho)=\rho$ in the original model, it was defined as:

$$f(\rho) = \rho_v + (1-\alpha_v)^n (\rho_l - \rho_v) \qquad n>1 \tag{12}$$

where the effect of vapor phase was added.

Cavitation model

The cavitation process is governed by the thermodynamics and the kinetics of the phase change dynamics occurring in the system. Equation 13 gives the conservation equation of vapor volume fraction. Here, the source terms $\dot{m}^+$ and $\dot{m}^-$, represent evaporation and condensation of the phases [3], respectively.

$$\frac{\partial \rho_v \alpha_v}{\partial t} + \nabla \cdot (\rho_v \alpha_v \vec{u}) = \nabla \cdot (\Gamma \nabla \rho_v \, \alpha_v/\rho) - \dot{m}^- + \dot{m}^+ \tag{13}$$

$$\dot{m}^+ = F_e \frac{3\alpha_{nuc}(1-\alpha_v)\rho_v}{R_B} \sqrt{\frac{2}{3}\frac{|P_v - P|}{\rho_l}} \tag{14}$$

$$\dot{m}^- = F_c \frac{3\alpha_v \rho_v}{R_B} \sqrt{\frac{2}{3}\frac{|P_v - P|}{\rho_l}} \tag{15}$$

Noting that Eqs. (14) and (15) are different from the original model proposed by Kubota et al. [3]. Since the evaporation rate is much higher than the condensation one- condensation usually occurs slowly and vaporization occurs quickly, different coefficients are imposed.

Further, several experimental studies have shown significant effect of turbulence on cavitating flows. Specifically, the incipient cavitation number increases with the turbulence intensity of the flow [21]. It seems that the local turbulent pressure fluctuation should be incorporated into the definition of the vapor pressure, so that the phase change responds to both thermodynamic and fluid dynamic conditions. In this study, we follow the model proposed by Singhal et al.[15]:

$$P_{turb} = 0.39 \rho k \tag{16}$$

$$P_v = (P_{sat} + P_{turb}/2) \tag{17}$$

This approach has been found to be simple and yield more favorable outcome (Singhal et al. [15]).

Grid, boundary and initial conditions

The two-dimensional computational domain is chosen to correctly follow the geometry of the experimental test section. An orthogonal mesh with 56,000 cells is generated as shown in Figure 7. Alternative meshe systems, with 41,540 and 65,580 cells, respectively, were also chosen to evaluate the grid sensitivity of the computation. Fig. 8 gives the grid distribution, finer mesh are located around the hydrofoil and the cavitating region as the experiments indicated, to obtain more accurate cavitating results. The nondimensional distance to solid walls y^+ is given between 20 and 50, which can satisfy the requirement of wall functions.

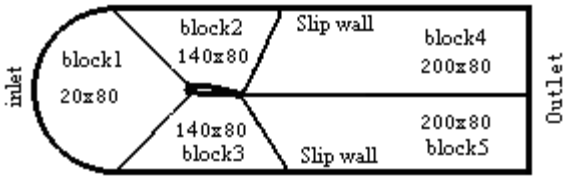

Figure 7: The schematic diagram of the dynamic measure system

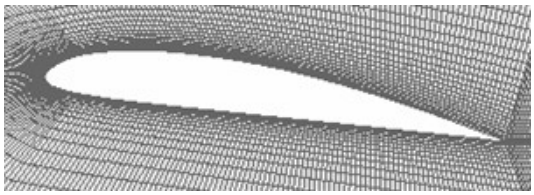

Figure 8: Computational grids around the hydrofoil

Table 1 shows the calculated lift/drag coefficients for all three meshes under no cavitation condition. In can be found that two results, computed with 56000 and 65580 cells, are similar basically. Considering the computational economy, 56000 cells are seclected as shown in Fig. 8.

Table. 1 *Cl* and *Cd* versus gird size

Gird size	$\sigma = 2.5$		$\sigma = 3$		EXP	
	Cl	*Cd*	*Cl*	*Cd*	*Cl*	*Cd*
41540	1.20	0.040	1.20	0.04		
56000	1.16	0.037	1.16	0.037	1.152	0.037
65580	1.14	0.04	1.14	0.04		

The numerical simulation conditions are adopted according to the experimental processes, as also shown in Fig. 7. In this study, the inflow streamwise velocity, volume fractions and turbulence quantities are specified at the inlet boundary, and the cross-sectional-averaged static pressure is imposed as the reference pressure at the outlet. A no-slip boundary condition is used at both the upper and lower walls. Also, the no-slip wall condition with a wall function is provided at the foil surface.

RESULTS AND DISCUSSIONS

The unsteady cavitating flow around a hydrofoil are investigated by joint experimental and numerical methods. The focus is on the discernible charactristics of cloud cavitaton, inclouding the unsteady dynamics, re-entrant jet generation, and the role of re-entrant jet in the sheding process of the cloud structures. In the results discussed below, the Reynolds number is fixed at value of 7×10^5, the attack angle $\alpha = 8^\circ$, and the cavitaton number $\sigma = 0.8$, while the upstream flow velocity U_{in}=10m/s.

Evolution of cloud cavittion patterns

Figure.9 presents one cycle aspects of the cloud cavity obtained by the experimental observation and numerical simulation respectively. The left ones result from visualizations. Fig 9(b) and Fig 9(c) present the void fraction and the flow

density evolution during one oscillation cycle predicted by the calculation respectively. Both the results obtained by observations and numerical simulations describe a quasi-periodic process of cloud cavitation development distinctly. When t=t0, immediately after a cavitating vortex shedding event takes place, a thin cavity occurs near the leading edge of the foil. The cavity grows with time, while traveling downstream. The cloud cavitating area consists of two parts: attached vapor sheet in the foreside of the cavity, and unsteady two-phase mixture in the rear region. When $t=t_0+16ms$, the cavity covers the whole suction surface of the foil, then it can be found a re-entrant jet is generated in the rear of cavity. The re-entrant jet runs from downstream to upstream. When $t=t_0+28ms$, the re-entrant jet reaches the attached sheet of the cavity, with the cavity break off two parts: attached vapor sheet in the foreside of the cavity, and unsteady two-phase mixture vortex structure in the rear region. Then the sheet cavity is compressed and begins to collapse, the two-phase mixture vortex structure flow downstream with a clockwise rotation. The rotating direction can be deduced by the influence of the main flow direction. The unsteady features of the cloud cavitation are changed periodically. The periodical vapor cloud shedding is mainly induced by the re-entrant jet.

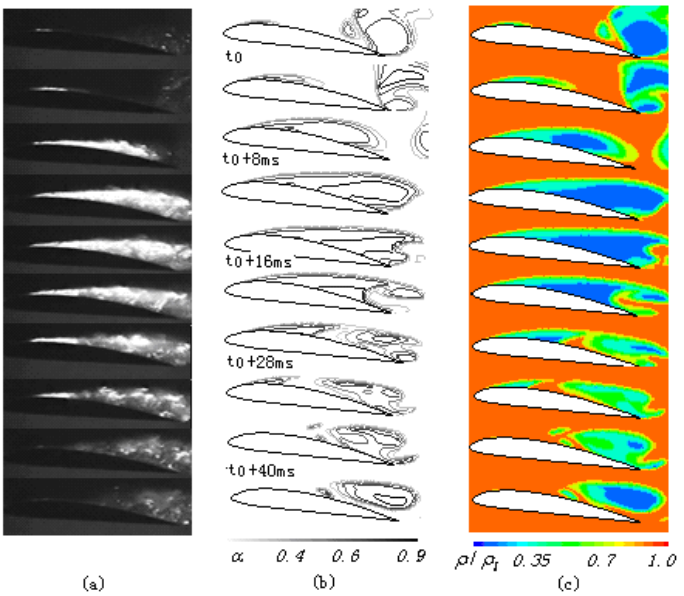

Figure 9: Time evolutions of the cavity shape ($\sigma = 0.8$ $\alpha = 8^{\circ}$)

Unsteady flow structure in the rear of a cloud cavity

Figure.10 indictes the pressure distribution around the foil in the progress of the two-phase mixture vortex structure flowing downstreamly. The time in the figure corresponds to Fig.9. It can be found that in $t=t_0+20ms$, the distribution on the suction surface of the foil is almost uniform, but there are gradient of pressure in the rear part of the cavity, and the cavity is unsteady in the area. When $t=t_0+24ms$, a local high pressure is generated in the middle of the cavity, which is followed with the cavity breaking off as mentioned above. The high pressure induces the condensation of vapor locally, and forms the breaking off of the cloud cavity. With the evolution of time, the high pressure area becomes large, and which induces the collapse of the attached vapor sheet in the foreside. It is clear that the raising of the local pressure is the main reason to lead the breaking off and shedding of the cloud structure. It should be pointed out that the high pressure is just located at the head of the re-entrant jet, as shown in Fig.9, that is, the raising of the local pressure is generated by the re-entrant jet. Fig.11 shows the time evolution of the pressure coefficient around the foil suction surface, and Fig.12 shows the contour plots of water vapor and velocity vectors around the foil at the corresponding time. The head of re-entrant jet at different time is marked in the Fig.12. It can be found that a local high pressure is generated by the re-entrant jet. The local pressure is just at the head of the re-entrant jet. When $t=t_0+28ms$, the maximal local pressure at point c can be found, which is corresponding to the cavity breaking off as shown in Fig.9. It is clear that the main reason for re-entrant jet to induce the shedding of the cloud cavity is the local high pressure at the head of the re-entrant jet.

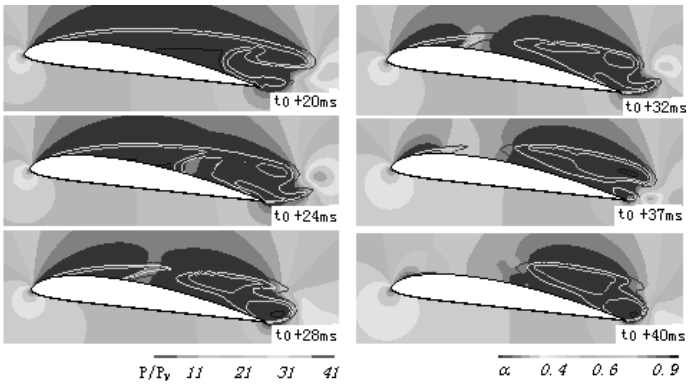

Figure 10: Pressure fields around the foil during the cavity breaking-off

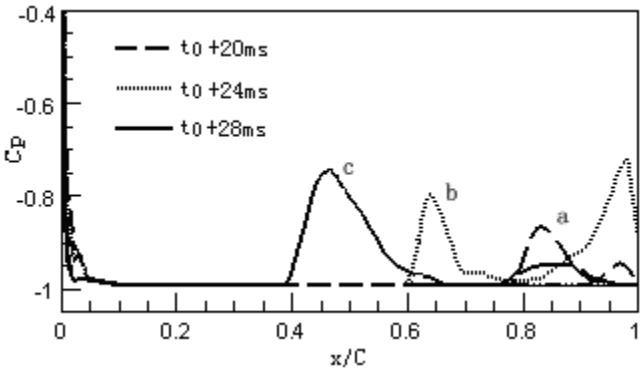

Figure 11: Time evolution of the Cp on the suction side

In order to know the behavior of the flow in the rear of the cloud cavity at the time when re-entrant jet is generated in detail, Fig.13 shows the time evolution of the pressure coefficient in line AB, which is located in the rear of the cavity. Fig.14 gives Time evolution of cavitating flow structure in the rear area of the foil. Fig.14 (a) is time evolution of cavitation patterns obtained by high-speed observation. Fig.14 (b) is time evolution of velocity vector distributions in the corresponding area obtained by the numerical simulation. It can be observed that the pressure gradient in the line AB is small at the stage of

cavity elongating as shown in Fig.13 when $t=t_0+13.8$ms. When the cavity covers the whole suction surface of the foil, there is distinct increasing for the pressure gradient, as shown when $t=t_0+16.2$ms. At the time, there is reverse flow which can observed at the rear of foil as shown in Fig.14. With the increasing of the pressure gradient, the reverse becomes stronger, and a re-entrant jet is generated as shown in Fig.14 when $t=t_0+17.8$ms. It can be concluded that the pressure gradient in the rear area of the foil is one of the reasons to induce the re-entrant jet.

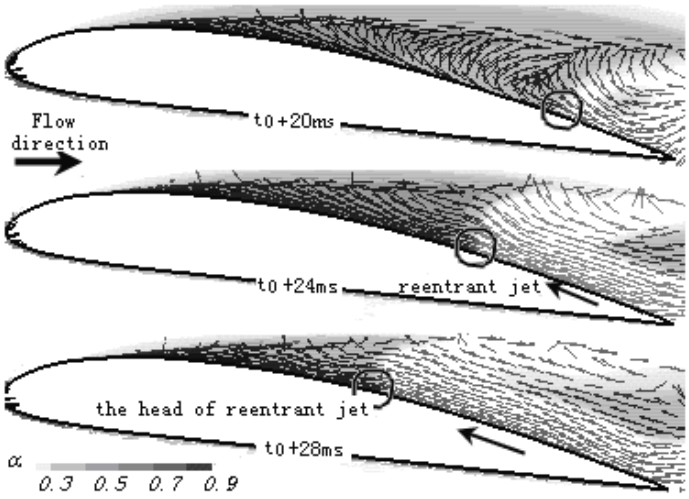

Figure 12: The contour plot of water vapor with corresponding velocity vector

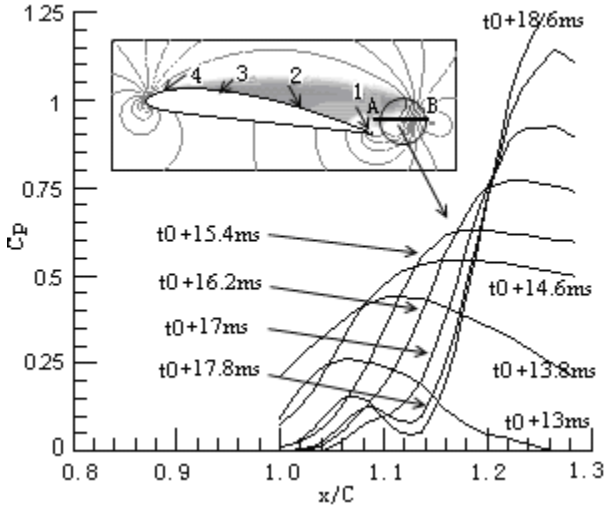

Figure 13: Time evolution of the C_p at the trail of the foil

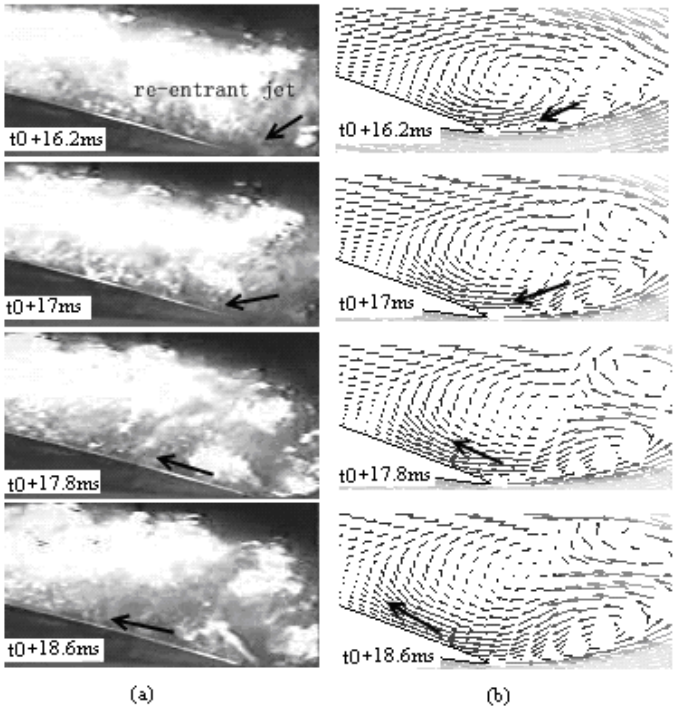

Figure 14: Time evolution of cloud cavitation in the rear area of the foil

Frequency characteristics of cloud cavitating

The frequency analysis of cloud cavitation pattern is also conducted. Fig.15 (a) presents the time evolution of cavity area obtained by experiment. The cavity area is defined the observed results on a laser beam sheet as shown in Fig.9 (a). Fig.15 (b) is the power spectral density of the cavity area obtained by FFT analysis. The cavity area changes with time periodically. The frequency is about 22Hz as which is corresponding to the shedding frequency of the cavity.

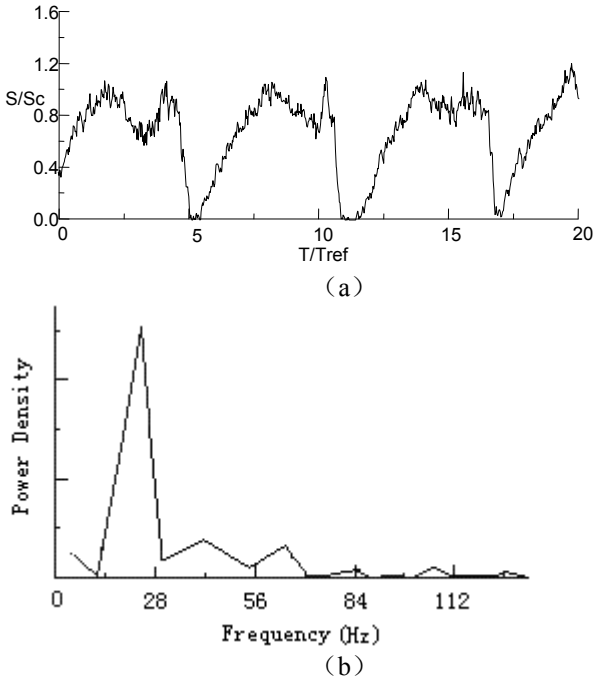

Figure 15: Power Spectral density of the cavity area

The evolutions of the lift coefficient obtained both by experiment and numerical simulation are presented in Figure16 (a). Figure 16(b) presents the power spectra density of the lift signal. A good good agreement is obtained between experimental data and numerical results. A strong spectral peak data occurs at a frequency f=22Hz. It is clear that the frequency of the cloud cavity shedding is equivalent to the frequency of lift coefficient.

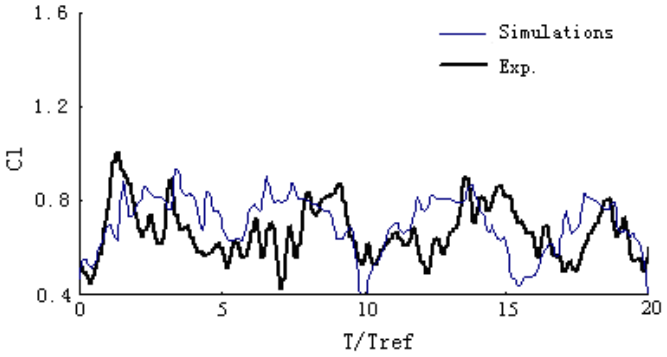

(a)

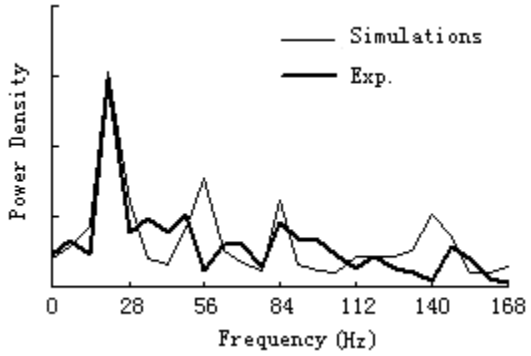

(b)

Figure 16: Power Spectral density of the lift coefficient

CONCLUSION

The cloud cavitation around a hydrofoil is investigated in this paper both numerically and experimentally. Following is a summary of the main findings:

(1) A good agreement is obtained between experimental data and numerical simulations, concerning both the quasi-periodic development process of cloud cavitation, the development of the re-entrant jet and main frequency of the lift acted on the foil.

(2) The cloud cavitating area is divided in two parts: attached vapor sheet in the foreside of the cavity, and unsteady two-phase mixture in the rear region, in the process of cavity breaking off, while the attached vapor sheet is compressed until to collapse, and the two-phase mixture vortex structure flow downstreamly with a clockwise rotation.

(3) The local high pressure at the head the re-entrant jet is the main reason to lead to sheding of the cloud cavity. There is a high pressure in the head of the re-entrant jet. With the running upstream of the jet, the high pressure increase until to break off the cavity.

(4) The adverse pressure gradient in the rear area of the cavity is mainly responsible for the generation of the re-entrant jet.

ACKNOWLEDGMENTS

The authors gratefully acknowledge support by the National Natural Science Foundation of China (NSFC, Grant No.: 50679001)

NOMENCLATURE

C	chord length of hydrofoil
Re	Reynolds number
n	empirical constant
S	bubble surface tension
U_∞	reference velocity
U	velocity component in x-direction
V	velocity component in y-direction
C_l	lift coefficient
C_d	drag coefficient
$\dot{m}^-$	condensation rate
$\dot{m}^+$	evaporation rate
σ	cavitation number
ρ	density of liquid-vapor mixture
ρ_l	density of liquid
ρ_v	density of vapor
C_l	lift coefficient
C_d	drag coefficient
$\sigma_{kRNG}, \sigma_{\varepsilon RNG}$	empirical constants
$C_{\varepsilon 1RNG}, C_{\varepsilon 2RNG}, C_{\mu RNG}$	empirical constants
F_e, F_c, α_{nuc}	empirical constants
P_{turb}	local turbulent pressure fluctuating
P_v	phase-change threshold pressure of vapor
P_B	pressure in the vapor bubble
P_∞	reference static pressure.
P_{sat}	saturated vapor pressure
K	turbulent kinetic energy
ε	turbulent dissipation rate
ν	kinematic viscosity
μ	liminar viscosity
μ_t	turbulent viscosity
R_B	vapor bubble radius
α_v	vapor volume fraction

REFERENCES

[1] Leroux, J B, Coutier-Delgosha, O. Astolfi, J A. 2005, "A joint experimental and numerical analysis of mechanisms associated to unsteady partial cavitation," *Phys. Fluids.* 17(5): 052101.

[2] Furness, R. A., and Hutton, S.P. 1975, "Experimental and Theoretical Study of Two-Dimensional Fixed-Type Cavities," *Journal of Fluids Engineering.* 97(4):515-522.

[3] Kubota, A., Kato,H. 1989, "Unsteady Structure Measurement of Cloud cavitation on a foil section using

conditional sampling techniques," *Journal of Fluids Engineering,* 111(3):204-210

[4] Le, Q., Franc, J. P., and Michel, J. M., 1993, "Partial Cavities: Pressure Pulse Distribution around Cavity Closure," ASME. *J. Fluids Eng*. 115(2).

[5] Kawanami Y, Kato H. 1997, "Mechanism and Control of Cloud Cavitation," *Journal of Fluids Engineering* 119(8): 788-794

[6] Callenaere M, Franc J P. 2001, "The cavitation instability induced by the development of a re-entrant jet," *J. Fluid Mech*. 444:223-256.

[7] Gopalan S. and Katz J. 2000, "Flow structure and modeling issues in the closure region of attached cavitation," *Phys Fluids.* 12: 895-911.

[8] Leroux J B, Astolfi J A， Billard J Y. 2001, "An experimental investigation of partial cavitation on a two-dimensional hydrofoil," *Fourth international symposium on cavitation,* SessionB1.002,

[9] Wang G Y., Senocak, I., Shyy W. 2001, "Dynamics of Attached Turbulent Cavitating Flows," *Progress in Aerospace Sciences,* 37(6): 551-581.

[10] Chen Y. and Heister S.D. 1994, "A numerical treatment for attached cavitation," *J Fluids Eng.* 116: 613-618.

[11] Wu J. Y., Wang G. Y., Shyy W. 2005, "Time-dependent turbulent cavitating flow computations with interfacial transport and filter-based models," Int J Numer Meth In Fluids. 49: 739-761.

[12] Delannoy Y., Kueny J.L. 1990, "Two phase flow approach in unsteady cavitation modeling," ASME *Fluids Eng Div Publ* FED, 98: 153-158.

[13] Senocak I., Shyy W. 2002, "Evaluation of cavitation models for Navier-Stokes computations," ASME *Fluids Eng Div Publ* , 257:395-401.

[14] Senocak I., Shyy W. 2004, "Interfacial dynamics-based modelling of turbulent cavitating flows, Part-1: model development and steady-state computations," *Int J Numer Methods Fluids*. 44: 975-995.

[15] Singhal A.K., Vaidya N., Leonard A.D. 1997, "Multi-dimensional simulation of cavitating flows using a PDF model for phase change," ASME *Fluids Eng Div* Publ FED.4: 7p

[16] Kunz R.F., Boger D.A., Stinbring D.R. 2000, "A preconditioned navier-stokes method for two-phase flows with application to cavitation prediction," *Comput Fluids*.29: 849-875.

[17] Coutier-delgosha O., Fertes-Patella R., Reboud J.L.2003, "Evaluation of the turbulence model influence on the numerical simulation of unsteady cavitation," *J Fluids Eng* Trans ASME. 125:38-45.

[18] Johansen S. T., Wu J.Y., Shyy W. 2004, "Filter-based unsteady RANS computations," *Int J Heat Fluid Flow.* 25: 10-21.

[19] Yuan W., Schnerr G.H. 2002, "Optimization of two-phase flow in injection nozzles-interaction of cavitation and external jet formation," *Proc. of ASME fluids engineering, Summer meeting*.

[20] Yakhot V., Orszag S.A., Thangam S., Gatski T.B., Speziale C.G. 1992, "Development of turbulence models for shear flows by a double expansion technique," *Phys Fluids A*.4: 1510-1520

[21] Keller A.P., Rott H.K. 1997, "Effect of flow turbulence on cavitation inception," ASME *Fluids Eng Div Publ* FED. 4: 3p.